Effect of an Organic Dicarboxylic Acid Salt on Fractionated Crystallization of Polypropylene Droplets

Y. Jin,* A. Hiltner, E. Baer

Department of Macromolecular Science and Engineering, Center for Applied Polymer Research, Case Western Reserve University, Cleveland, Ohio 44106

Received 27 December 2006; accepted 10 January 2007
DOI 10.1002/app.26584
Published online 24 May 2007 in Wiley InterScience (www.interscience.wiley.com).

ABSTRACT: The effect of a particulate nucleating agent on fractionated crystallization of polypropylene (PP) was studied. A novel method utilizing breakup of PP nanolayers was used to obtain a dispersion of PP droplets in a polystyrene (PS) matrix. An assembly with hundreds of PP nanolayers alternating with thicker PS layers was fabricated by layer-multiplying coextusion. The concentration of an organic dicarboxylic acid salt (HPN) nucleating agent in the coextruded PP nanolayers was varied up to 2 wt %. When the assembly was heated into the melt, interfacial driven breakup of the thin PP layers produced a dispersion of PP particles in a PS matrix. Analysis of optical microscope images and atomic force microscope images indicated that layer breakup produced a bimodal particle size distribution of submicron particles and large, micron-sized particles. Almost entirely submicron particles were obtained from breakup of 12 nm PP layers. The fraction of PP as submicron particles dropped dramatically as the PP nanolayer thickness increased to 40 nm. Only large, micron-sized particles were obtained from 200 nm PP nanolayers. The crystallization behavior of the particle dispersions was characterized by thermal analysis and wide angle X-ray diffraction. Only part of the PP was nucleated by HPN. It was found that HPN was not effective in nucleating the population of submicron particles. The particulate HPN was too large to be accommodated in the submicron PP particles. On the other hand, the amount of nucleated crystallization qualitatively paralleled the fraction of PP in the form of large, micron-sized particles. © 2007 Wiley Periodicals, Inc. J Appl Polym Sci 105: 3260–3273, 2007

Key words: polypropylene; nucleating agents; fractionated crystallization; nucleation

INTRODUCTION

Nucleating agents are added in crystalline polymers to increase the rate of crystallization during molding and extrusion processes. These agents increase the nucleation rate by acting as heterogeneous nuclei. In the case of isotactic polypropylene (PP), the use of nucleating agents is particularly important owing to its relatively low rate of crystallization. Moreover, this polymer is particularly amenable to nucleation. With a sufficiently active nucleating agent, PP can be made transparent. A large number of compounds have been reported to nucleate the α-form of PP.[1–6] The nucleating agents are categorized into two types: (1) those that are dispersed in the polymer and remain as a solid particulate in the polymer melt, examples include organic dicarboxylic acid salts[7]; and (2) those that dissolve in the polymer melt and phase separate during cooling to produce the heterogeneous nuclei, examples are sorbitol and its derivatives.[8]

One approach to studying nucleation of PP is through the crystallization of dispersed particles. Typically, the particles exhibit multiple crystallization exotherms. This phenomenon, known as fractionated crystallization, arises when the particles are too numerous for each to contain one or more of the most active nuclei.[9–12] Each of the exotherms represents a population of particles whose crystallization is nucleated by a different heterogeneity that is activated at a different supercooling. There is an opportunity to probe the activity of heterogeneous nucleating agents through their effect on fractionated crystallization. Nucleated PP is included in only a few studies of fractionated crystallization.[13,14] Although the results are very limited in scope, they confirm that this could be a promising approach.

We recently demonstrated a method based on breakup of PP nanolayers for obtaining a dispersion of submicron PP particles in a PS matrix without the need for a compatibilizing agent.[15,16] This has the advantage of minimizing the interaction between the particles and the matrix. Layer-multiplying coextrusion is used to fabricate assemblies in which PP

Correspondence to: A. Hiltner (pah6@cwru.edu).
**Present address:* The Dow Chemical Company, Freeport, Texas 77541.

Contract grant sponsor: NSF Science and Technology Center for Layered Polymeric Systems; contract grant number: 0423914.

© 2007 Wiley Periodicals, Inc.
WILEY InterScience® DISCOVER SOMETHING GREAT

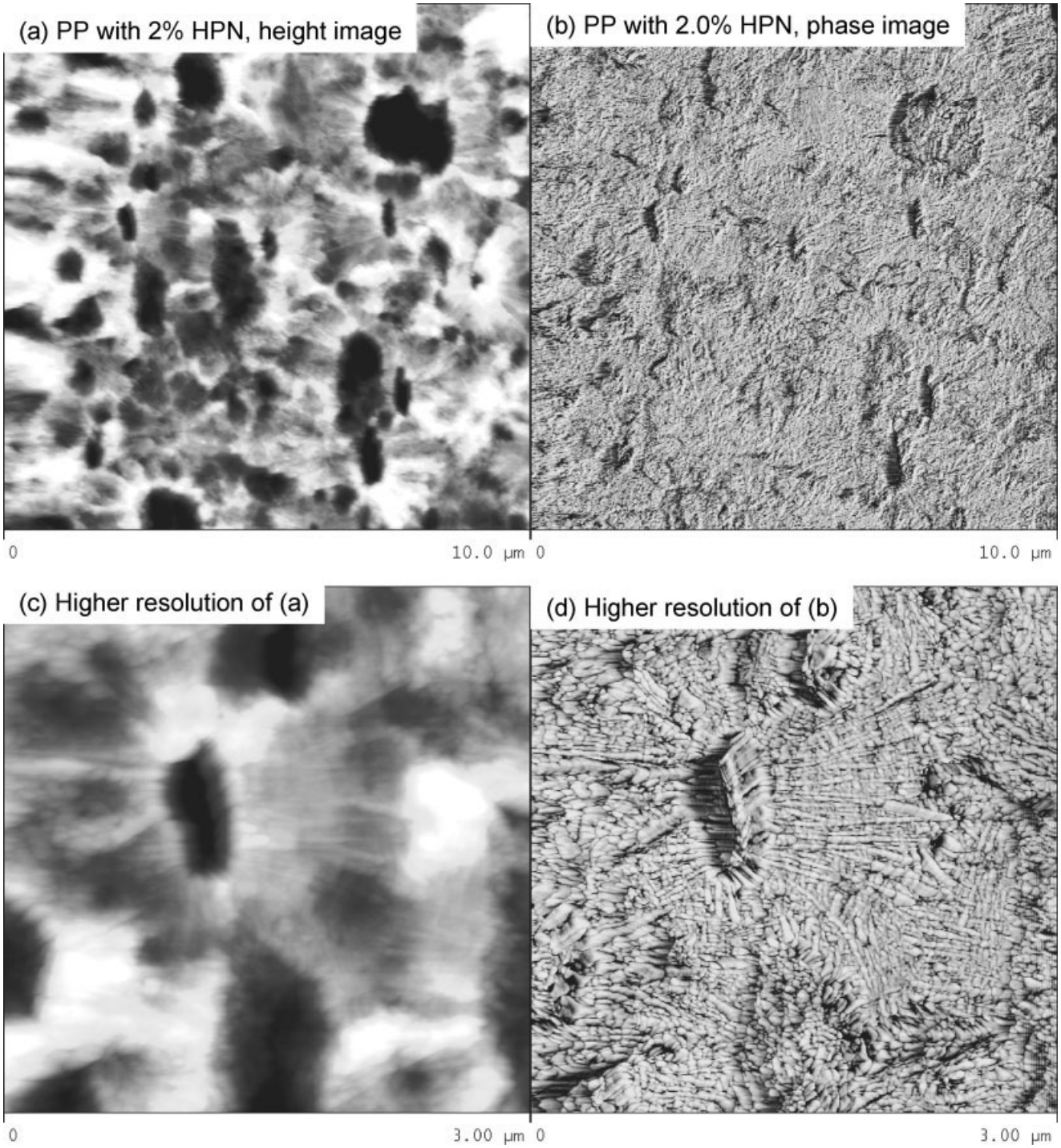

Figure 1 AFM images of PP with 2.0% HPN after the microtomed surface was etched to remove the HPN particles: (a) Height image; (b) phase image; (c) higher resolution of (a); and (d) higher resolution of (b).

nanolayers alternate with thicker polystyrene (PS) layers. When the assembly is heated into the melt, the PP nanolayers break up to form a dispersion of PP droplets in a PS matrix. Upon cooling, the droplets solidify as PP particles. The nature of the breakup process produces a bimodal distribution with one population of submicron particles and a second population of large micron-sized particles.[17] The particle size distribution is controlled by the thickness of the PP nanolayer. A distribution that contains almost entirely submicron particles is obtained by breakup of 12 nm PP layers. The fraction of PP as submicron particles drops dramatically as the layer thickness increases to 40 nm. Only the submicron particles crystallize by homogeneous nucleation in the smectic form. Fractionated crystalli-

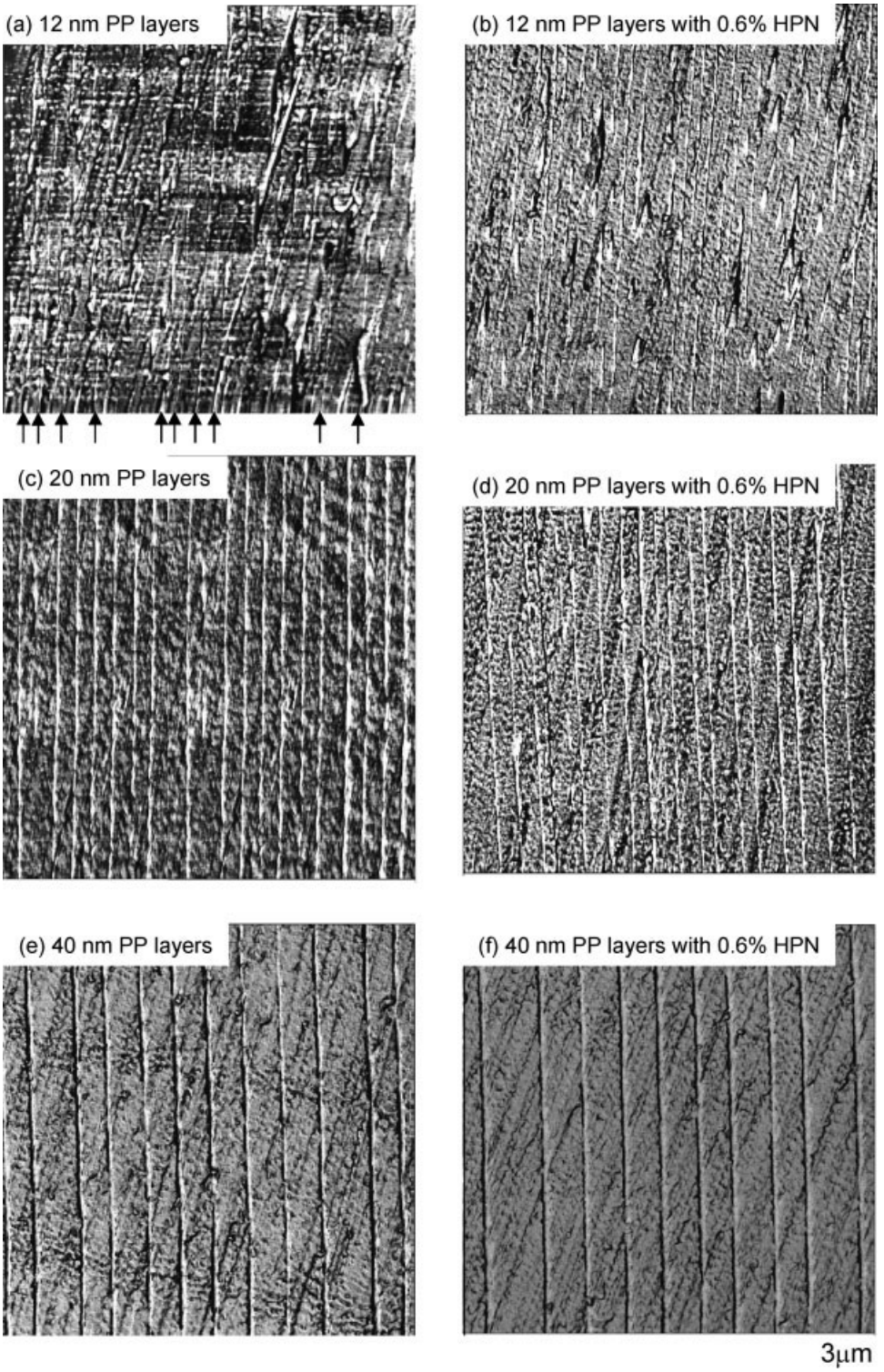

Figure 2 AFM phase images of the cross sections from coextruded nanolayer assemblies: (a) 75 μm film with 12 nm PP layers; (b) 75 μm film with 12 nm PP layers containing 0.6% HPN; (c) 125 μm film with 20 nm PP layers; (d) 125 μm film with 20 nm PP layers containing 0.6% HPN; (e) 250 μm film with 40 nm PP layers; and (f) 250 μm film with 40 nm PP layers with 0.6% HPN.

zation of the large micron-sized particles in the PP α-form results in multiple exotherms.

In the present study, this novel methodology was used to investigate heterogeneous nucleation of PP. A commercial nucleating agent was added to the PP resin prior to coextrusion as layered assemblies. The crystalline organic dicarboxylic acid salt remained as a solid particulate in the melt and provided a low

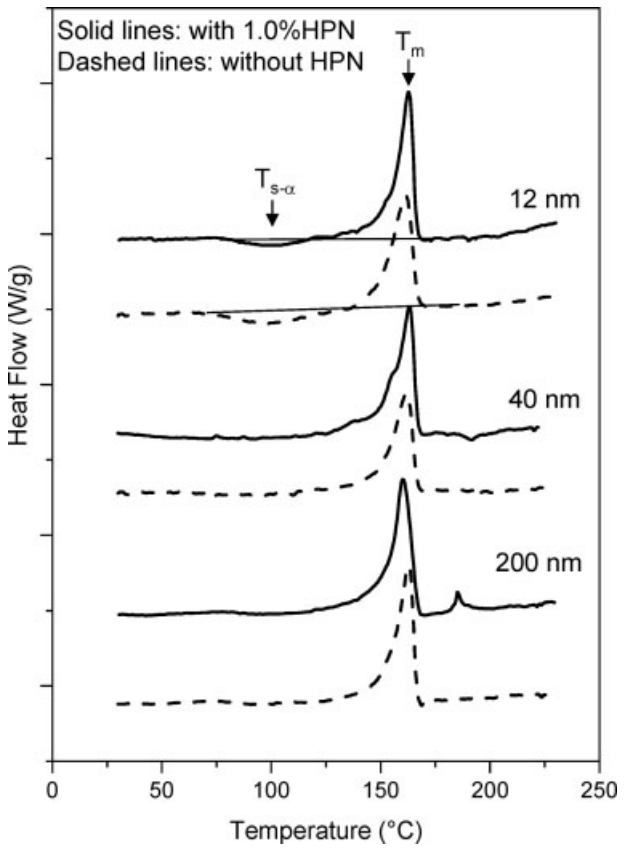

Figure 3 Heating thermograms of the coextruded nanolayer assemblies. The PP nanolayer thickness is indicated.

energy surface for crystallization during cooling. The effect of the nucleating agent on homogeneous nucleation of the submicron PP particles and on fractionated crystallization of the large, micron-sized particles was examined.

MATERIALS AND METHODS

The isotactic polypropylene (PP) was Dow ZN5D98 with bulk density 0.900 g cm^{-3} according to ASTM D 792 and melt flow index of 3.4 g/10 min according to ASTM D1238. The polystyrene (PS) was Dow STYRON 685D with bulk density 1.040 g cm^{-3} according to ASTM D 792 and melt flow index of 1.5 g/10 min according to ASTM D1238. The nucleating agent was Milliken Hyperform HPN-68L (HPN).

The nucleating agent was added to PP by blending in a Haake Rheomix 600 twin screw extruder with barrel temperature set at 230°C. A master batch with 10 wt % HPN was prepared. The master batch was further blended with PP to the target concentrations of 0.1, 0.3, 0.6, 1.0, and 2.0 wt % HPN and palletized.

The nucleated PP was coextruded into a layered assembly with 257 alternating layers of PP and PS in a PP/PS 10/90 composition as described previously.[16,17] The final film thickness was varied by controlling the take-off speed between 1 and 20 feet min^{-1}. The nominal thickness of the PP layers calculated from the composition and the film thickness ranged from 12 to 200 nm. Films of PS were also extruded for controls. To examine layer uniformity, the films were embedded in epoxy, sectioned through the cross section, and examined in the AFM as described previously.[16,17]

The PP nanolayers were broken up into droplets by heating the assembly in the DSC to 230°C at a rate of 10°C min^{-1} and holding it at that temperature for 3 min before cooling at a rate of 10°C min^{-1}. The heating thermogram of the PS control film was obtained with the same heating rate. The heating curve of PS was normalized to the weight composition of the assembly and subtracted from the thermogram of the assembly to isolate the PP peaks from the superimposed glass transition of PS.

To obtain a representative population of PP particles for size analysis, the PS matrix was selectively dissolved in toluene and the resulting suspension of PP particles was dried on a slide to obtain a thin PS film containing PP particles.[17] Subsequent characterization of the broad PP particle size distribution required the use of both lower magnification OM images and higher resolution AFM images.

Heating thermograms of the PP particles dispersed in the PS matrix were obtained at 40°C min^{-1}. A PS control film was subjected to the same thermal history as the nanolayer assembly and similarly characterized by thermal analysis. The heating and cooling curves of PS were normalized to the weight composition of the assembly and subtracted from the thermogram of the assembly. The enthalpy of each peak was normalized by weight to 100% PP. Crystallinity was calculated using 210 J g^{-1} as the PP heat of melting.[18,19]

The wide angle X-ray diffraction (WAXD) pattern of the PP particles dispersed in the PS matrix was obtained at ambient temperature in the transmission mode as described previously.[16,17]

TABLE I
Melting Enthalpies of PP Nanolayers

PP nanolayer thickness	$\Delta H_{s-\alpha}$ (J/g)	ΔH_m (J/g)	X_s[a] (%)	X_{total}[b] (%)
12 nm	−13	63	28	30
12 nm with 1.0% HPN	−10	64	22	30
40 nm	0	63	0	30
40 nm with 1.0 % HPN	0	70	0	33
200 nm	0	67	0	32
200 nm with 1.0% HPN	0	77	0	37

[a] Calculated from $\Delta H_{s-\alpha}$ with $\Delta H^0_{s-\alpha} = -46$ J/g.
[b] Calculated from ΔH_m with $\Delta H^o_m = 210$ J/g.

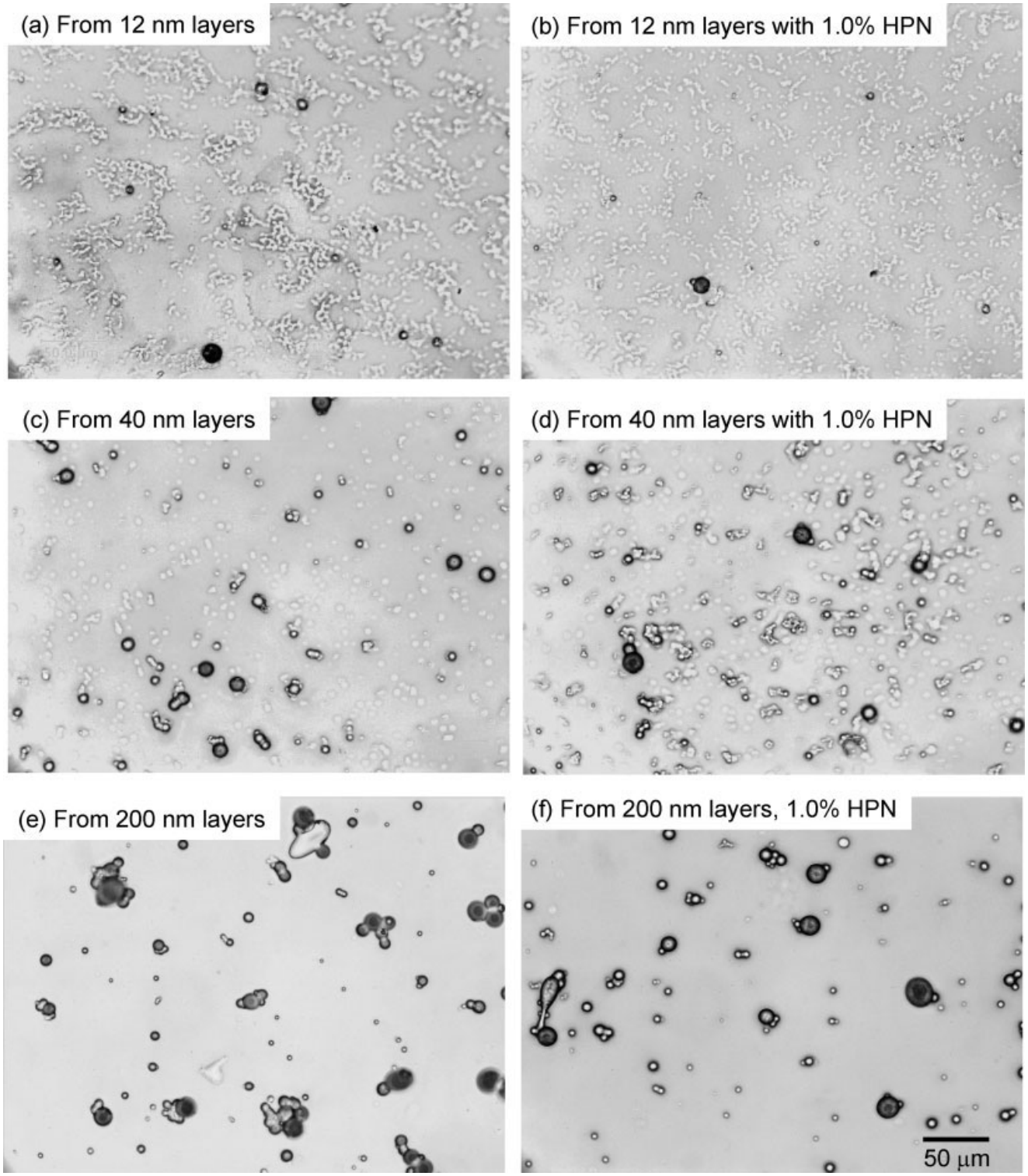

Figure 4 OM images of the PP particles from: (a) 12 nm layers; (b) 12 nm layers with 1.0% HPN; (c) 40 nm layers; (d) 40 nm layers with 1.0% HPN; (e) 200 nm layers; and (f) 200 nm layers with 1.0% HPN.

RESULTS AND DISCUSSION

Nucleated crystallization of PP by HPN

The nucleating effect of HPN was characterized by the crystallization temperature and crystallization enthalpy of PP. Addition of only 0.1% HPN increased the crystallization temperature from 110 to 128°C. Further addition of HPN to 2.0% increased the crystallization temperature by only a couple more degrees. The crystallization enthalpy also increased, but only slightly from 84 J g^{-1} for PP to 89 J g^{-1} for PP with 2.0% HPN.

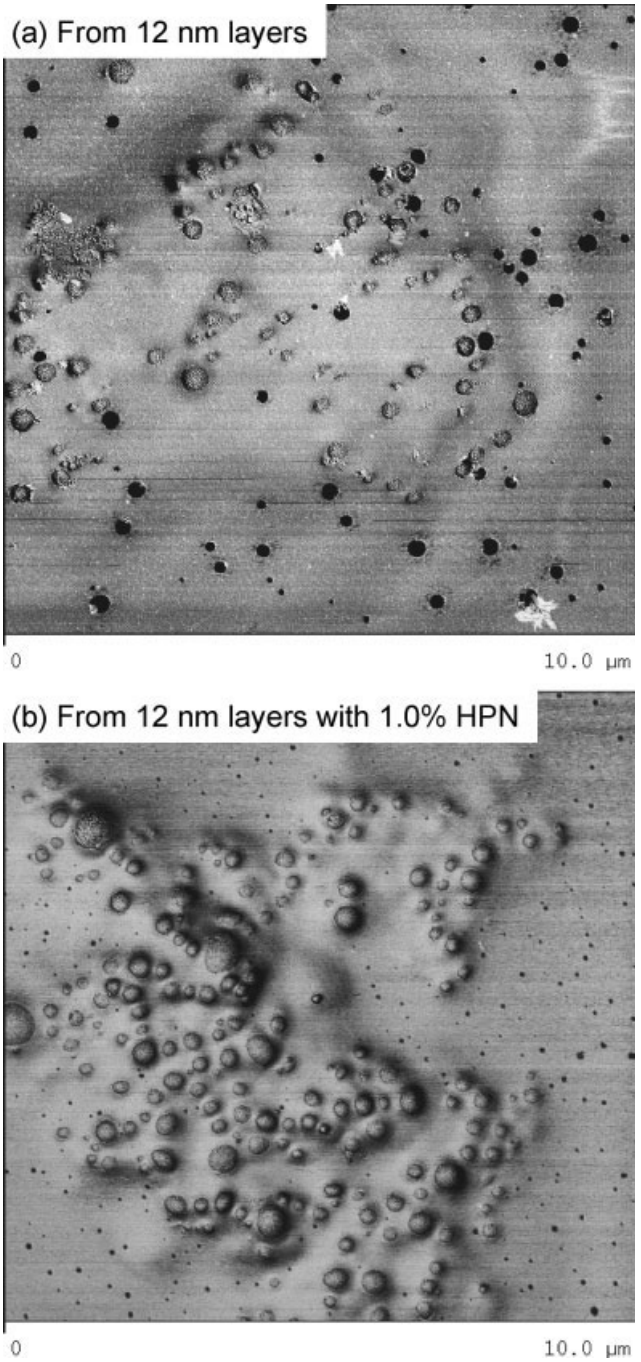

Figure 5 AFM images of the PP particles from: (a) 12 nm layers; and (b) 12 nm layers with 1.0% HPN.

The AFM images of PP with 2.0% HPN after the specimen was microtomed and etched showed numerous platelet-shaped depressions where the HPN was selectively etched away, Figure 1. The depressions left by the etched platelets, which were more apparent in the height images than in the phase images, were generally 0.5–1.0 μm in length. In higher resolution phase images, it was possible to see where etching away the HPN revealed the highly ordered lamellar structures that nucleated from the surface of the HPN platelet.

Polypropylene nanolayers with HPN

Coextrusion of thin PP layers with alternating thick PS layers resulted in the layered structures shown in cross section in Figure 2. The presence of the HPN nucleating agent did not affect layer thickness and integrity as seen by the correspondence in the cross sections of films with and without HPN. Very thin PP layers were sandwiched between thick PS layers. In films with 12 nm PP layers, the PP layers (arrows) had a tendency to pullout during microtoming, which made it difficult to measure individual layer thicknesses. However, the 125 nm layering periodicity matched the combined PP and PS layer thicknesses predicted from the total assembly thickness and the number of layers. Thus all the layers were accounted for, although it appeared that some of the layers were not continuous but contained breaks due to interfacial instability. In films with 20 and 40 nm PP layers, uniform and continuous PP nanolayers were clearly present. The layering periodicities of 200 nm in the former and 400 nm in the latter matched the calculated periodicities. Films with thicker PP layers also exhibited uniform, continuous layers.

The heating thermograms of nucleated PP nanolayers are compared with the heating thermograms of unnucleated PP nanolayers in Figure 3. The 12 nm layers showed the main melting peak together with a broad premelting exotherm at about 100°C. The exotherm was previously identified with the transformation of the smectic form to the usual α-form of PP.[16] The enthalpy of the smectic to α-form transformation, and the melting enthalpy of the PP α-form were about the same for both nucleated and unnucleated nanolayers, Table I, which indicated that the HPN did not nucleate crystallization of PP confined as 12 nm layers.

The smectic to α-form transformation was not observed in the heating thermograms of 40 nm layers. The melting enthalpy of the nucleated 40 and 200 nm PP layers was somewhat higher than that of the unnucleated layers, Table I. However, for both nucleated and unnucleated PP nanolayers, the melting enthalpy was significantly lower than the melting enthalpy of the bulk resin. Thus, although HPN appeared to have some nucleating effect on 40 and 200 nm layers, the influence of confinement remained and the HPN did not nucleate complete crystallization of the PP to the level achieved in the bulk resin.

Polypropylene particles produced by layer breakup

Heating to 230°C transformed the appearance of the films from transparent to opaque. When the films

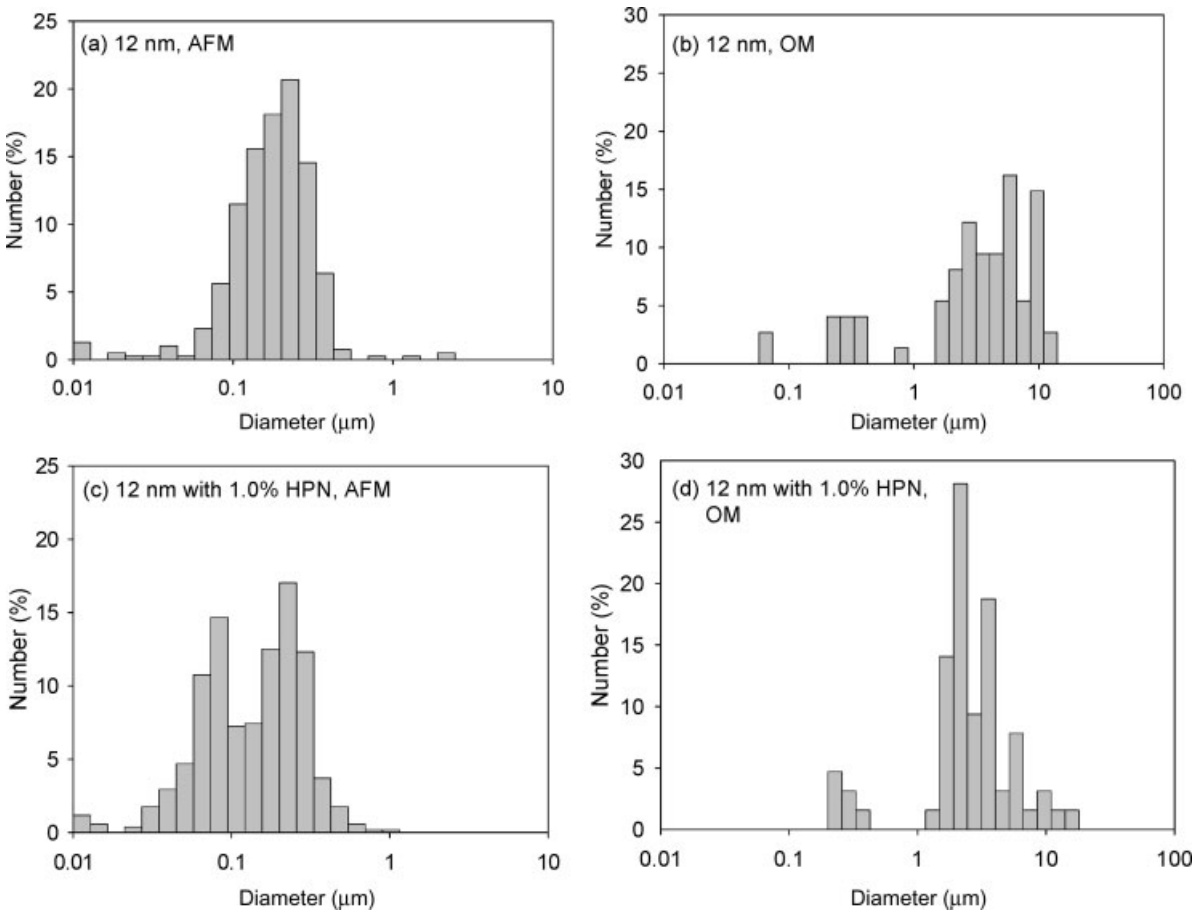

Figure 6 Particle size distributions from 12 nm layers: (a) Submicron PP particles from AFM images; (b) large PP particles from OM images; (c) submicron PP particles with 1.0% HPN from AFM images; and (d) large PP particles with 1.0% HPN from OM images.

were taken into the melt, interfacial-driven breakup transformed the PP nanolayers into droplets. Upon cooling, the droplets solidified as PP particles dispersed in the PS matrix. To obtain a representative population of particles, the PS matrix was selectively dissolved in toluene and the resulting suspension of PP particles was dried on a slide to obtain a thin PS film containing PP particles. The OM images of the PS films in Figure 4(a,b) compare the particles from 12 nm films without HPN and with 1.0% HPN. Both images show a few large particles and many smaller particles that are out of focus. Typical optical micrographs of particles from 40 nm layers showed mostly large particles and only a few out-of-focus small particles, Figure 4(c,d). Only large particles were seen in the optical micrographs of particles from 200 nm layers, Figure 4(e,f). From a visual inspection of the OM images, there were no discernable differences between the particles from PP layers without nucleating agent and from the layers that contained 1.0% HPN.

The AFM images in Figure 5(a,b) show the particles from 12 nm layers at much higher resolution. The images revealed a high concentration of bright, submicron particles. Again, from a visual inspection of the images, there were no obvious differences in the particle sizes from unnucleated PP nanolayers and from nanolayers that contained 1.0% HPN.

The bimodal particle size distribution from 12 nm layers was obtained by combining the lower magnification OM images with the higher resolution AFM images. The many small particles in AFM images ranged in size from 20 nm to about 0.5 mm, with the distribution centered at about 0.2 mm, Figure 6(a). Of the 800 particles measured in the AFM images, only four were larger than 0.5 μm. The broad size distribution of the few large particles was taken from the optical micrographs, Figure 6(b). The smallest particles that were included in this analysis were about 0.5 μm.

The distribution of submicron particles obtained from 12 nm layers that contained 1.0% HPN was similar to that from 12 nm layers without HPN, but was broadened somewhat toward smaller particles, Figure 6(c). The distribution of large particle sizes from 12 nm layers with 1.0% HPN was sharper than that from 12 nm layers without HPN and was centered at about 3 μm, Figure 6(d). However, consider-

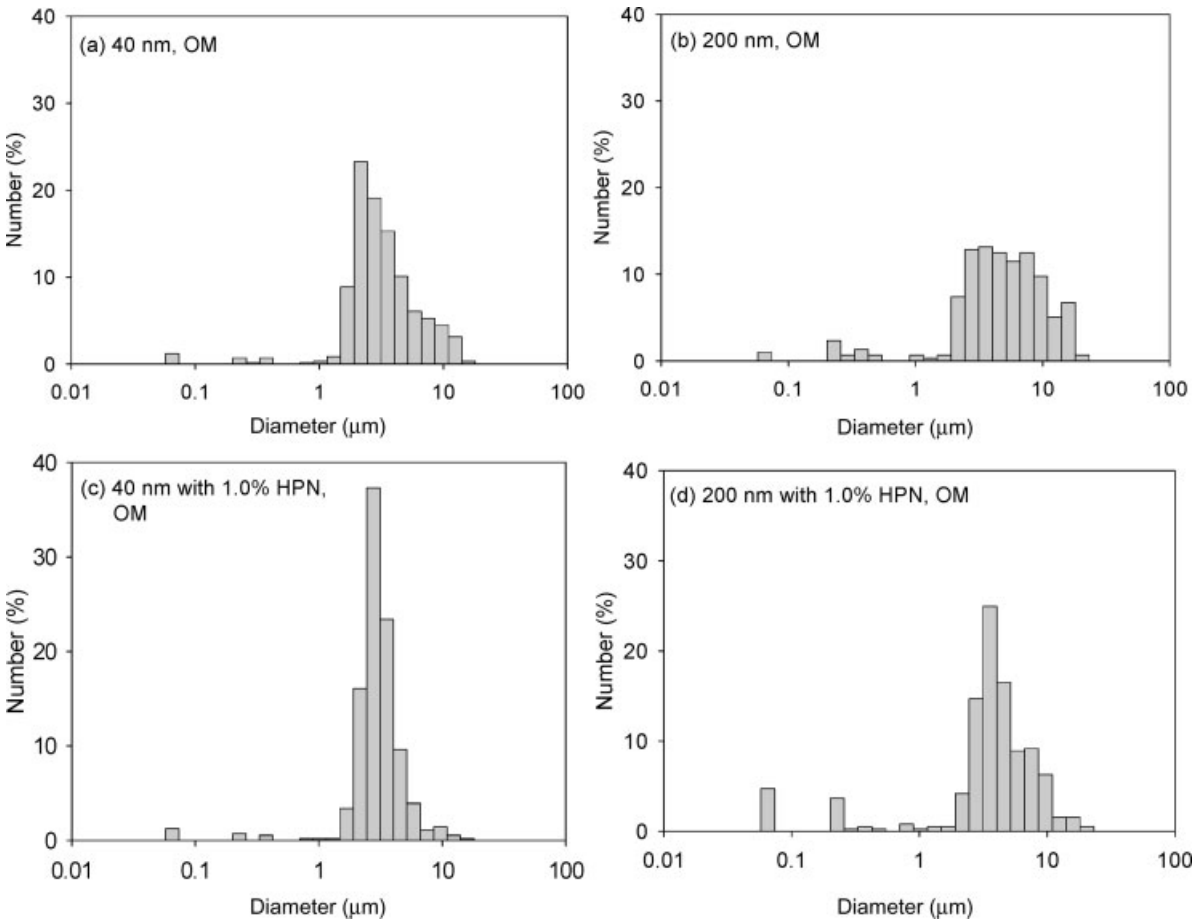

Figure 7 Large particle size distributions from OM images: (a) From 40 nm PP layers; (b) from 200 nm PP layers; (c) from 40 nm PP layers with 1.0% HPN; and (d) from 200 nm layers with 1.0% HPN.

ing the small number of particles, the distributions were not thought to be significantly different. In both unnucleated and nucleated PP, the largest particle was a rare one of about 15 μm.

The large particles dominated the volume distribution from 40 and 200 nm layers. The OM images of particles from 40 nm layers suggested that only a few percent of the PP was in the form of submicron particles. Only large particles were observed from the 200 nm layers. The distributions were somewhat sharper in particles obtained from layers with 1.0% HPN, however the sizes were about the same, Figure 7. In both cases, the distribution from 200 nm layers was substantially broadened towards larger particles.

The relative volume fractions of large and small particles from 12 nm layers were estimated by combining the OM images, which sampled a large area of the film thickness, with the AFM images which sampled a small area of the film surface, as described previously.[17] The particle distributions were normalized by area and thickness, and converted to volume distributions, Figure 8. The figure clearly revealed the bimodal distribution in particle sizes from 12 nm layers. Approximately 90% of the PP was in the form of submicron particles. The presence of HPN in the PP layers did not appear to significantly affect the bimodal particle size distribution. The volume distributions for particles from 40 and 200 nm layers were also not significantly affected by HPN. In both cases, the broad distribution shifted toward larger particles as the layer thickness increased from 40 to 200 nm.

Crystallization and melting of particles from 12 nm layers

The crystallization and melting thermograms of the particles from 12 nm PP layers with various amounts of HPN are shown in Figure 9. Without nucleating agent in the PP, the primary crystallization exotherm appeared at about 40°C with a much smaller peak at about 60°C. The enthalpies were -42.2 J g^{-1} for the 40°C peak and -4.5 J g^{-1} for the 60°C peak, Table II. In a previous report,[17] the 40°C peak was identified as homogeneous nucleation of the PP smectic form and the 60°C peak with crystallization of a highly defective α-form. Even with 1.0% HPN in the PP, crystallization occurred primarily at 40 and 60°C.

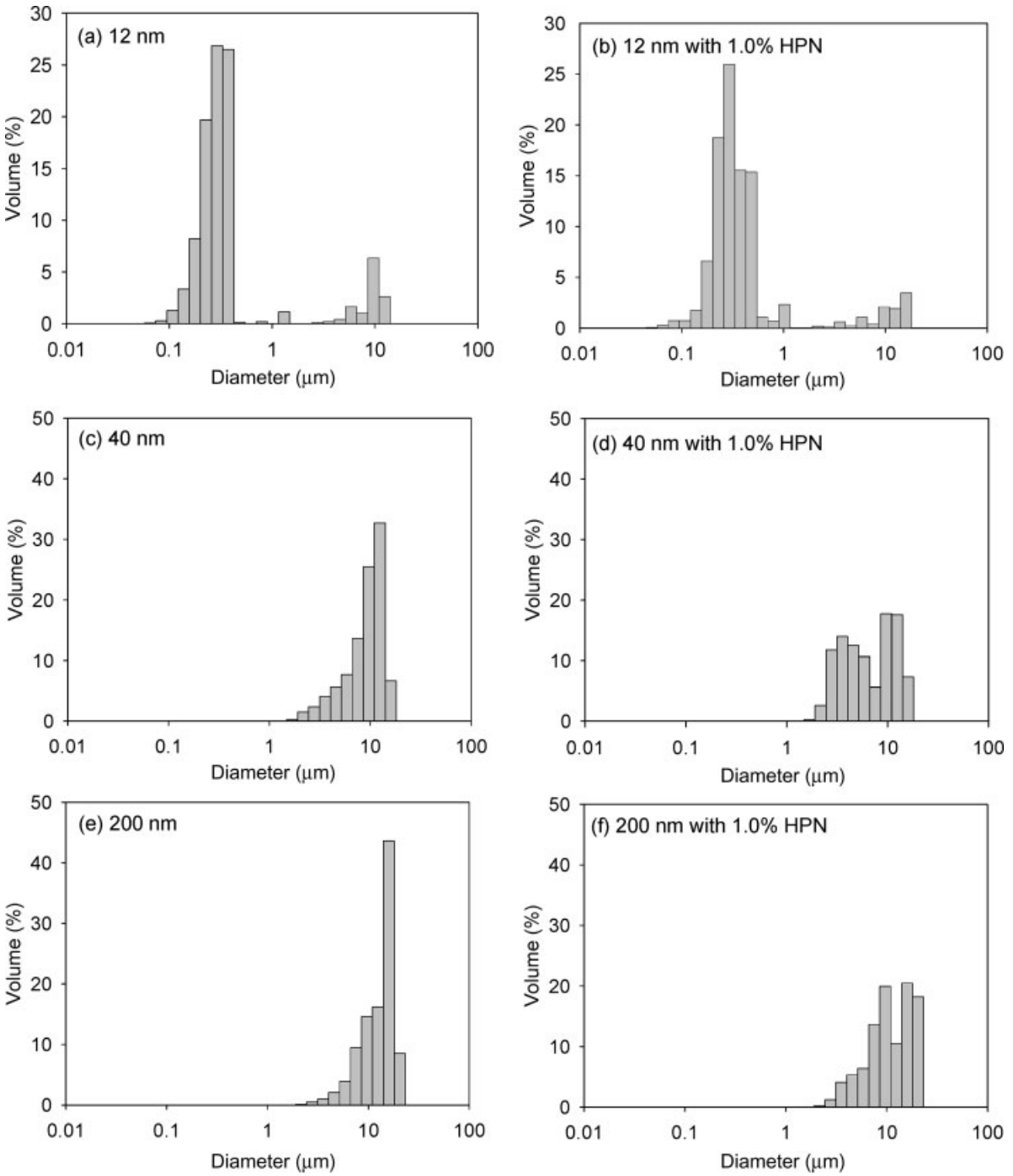

Figure 8 Particle volume distributions: (a) From 12 nm PP layers; (b) from 12 nm PP layers with 1.0% HPN; (c) from 40 nm PP layers; (d) from 40 nm PP layers with 1.0% HPN; (e) from 200 nm PP layers; and (f) from 200 nm PP layers with 1.0% HPN.

The principal effect of HPN was to slightly decrease the enthalpy of the 40°C peak and slightly increase the enthalpy of the 60°C peak. The amount of smectic PP crystallinity calculated from the enthalpy of the 40°C exotherm using $\Delta H_s^0 = 164$ J g^{-1} decreased steadily from 26% in PP particles that did not contain a nucleating agent to 18% in particles with 1.0% HPN, Table II. The amount of defective α-form crystallinity calculated from the 60°C peak increased from 2% in PP particles to 9% in particles with 1% HPN. Thermograms of particles with 1.0% HPN included a small crystallization exotherm at 125°C corresponding to HPN-nucleated crystallization. However, the small enthalpy, less than 2 J g^{-1}, indicated that only about 1% of the PP crystallized in this manner.

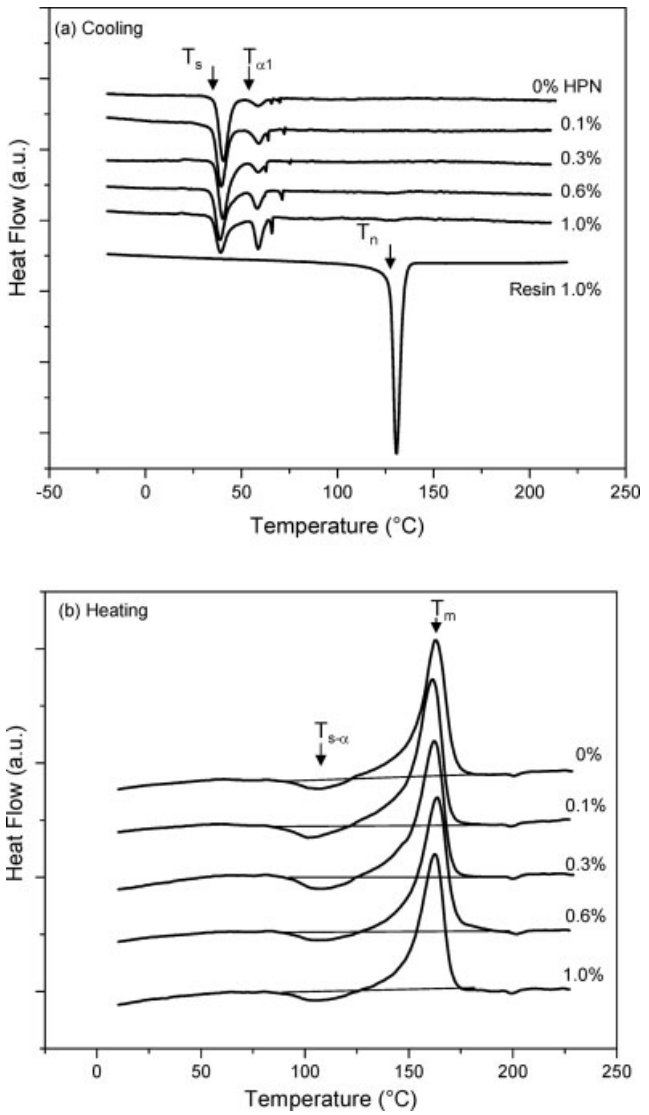

Figure 9 Thermograms of the PP/PS assembly with 12 nm PP layers containing various concentrations of HPN after heating to 230°C: (a) Cooling thermograms; and (b) subsequent heating thermograms. The PS contribution was subtracted.

The subsequent heating thermograms exhibited a broad exotherm at about 100°C, which was the transformation of smectic PP to the α-form,[20,21] and an endotherm at 164°C, which was the melting of α-form PP. With increasing HPN, the enthalpy of the smectic transformation decreased, Table III. Using values of $\Delta H^0_{s-\alpha} = -46$ J g^{-1} and $\Delta H^0_s = 164$ J g^{-1} acquired previously,[17] the amount of smectic phase that underwent the transformation to α-form during heating (X_s in Table III) coincided with the amount of smectic phase that crystallized at 40°C during cooling (X_s in Table II).

The total crystallinity was obtained from the enthalpy of the α-form melting peak in the heating thermogram (X_{total} in Table III) and, alternatively, from the cooling thermogram by summing the amount of smectic form crystallinity and the amount of α-form crystallinity (X_{total} in Table II). Both approaches gave the same result. Moreover, the total crystallinity did not change with addition of HPN, but remained constant at about 27%. This was considerably lower than the crystallinity of the HPN-nucleated PP resin, which was about 42%.

The WAXD patterns from the particle dispersions are compiled in Figure 10. The diffraction pattern of particles with up to 0.3% HPN had only the two broad peaks of smectic PP at 15° and 21° and did not include any of the PP α-form reflections. In particles with 0.6% HPN or more, very weak reflections characteristic of the PP α-form appeared, superimposed on the broad reflections of the smectic form. This was consistent with the previous interpretation that the smectic form crystallized at 40°C whereas a defective α-form crystallized at 60°C.[17]

Crystallization and melting of particles from 20, 40, and 200 nm layers

Fractionated crystallization of unnucleated PP from 20 nm layers resulted in exotherms at 40 and 60°C, corresponding to crystallization of the smectic form and the defective α-form, respectively, and a smaller exotherm at 85°C, Figure 11(a). Compared to crystallization of particles from the 12 nm layers, the enthalpy of the 40°C peak was substantially lower and the enthalpy of the 60°C peak was substantially higher. Nevertheless, the total crystallization enthalpy

TABLE II
Crystallization Enthalpies of PP Particles from 12 nm Layers

HPN (wt %)	ΔH_s at 40°C (J/g)	$\Delta H_{\alpha 1}$ at 60°C (J/g)	ΔH_n at 126°C (J/g)	X_s[a] (%)	X_α[b] (%)	X_{total}[c] (%)
0.0	42.2	4.5	0	26	2	28
0.1	36.3	10.2	0	22	5	27
0.3	38.4	7.8	0	23	4	27
0.6	35.6	10.5	1.67	22	6	28
1.0	30.1	16.3	1.89	18	9	27

[a] Calculated from ΔH_s with $\Delta H^0_s = 164$ J/g.
[b] Calculated from $\Delta H_{\alpha 1} + \Delta H_n$ with $\Delta H^0_\alpha = 210$ J/g.
[c] Equal to $X_s + X_\alpha$.

TABLE III
Melting Enthalpies of PP Particles from 12 nm Layers

HPN (wt %)	$\Delta H_{s-\alpha}$ at 106°C (J/g)	ΔH_m at 162°C (J/g)	X_s [a] (%)	X_{total} [b] (%)
0	−12.0	59.2	26	28
0.1	−10.1	57.2	22	27
0.3	−10.9	58.0	24	28
0.6	−9.2	59.1	20	28
1.0	−8.5	58.2	18	28

[a] Calculated from $\Delta H_{s-\alpha}$ with $\Delta H^0_{s-\alpha} = -46$ J/g.
[b] Calculated from ΔH_m with $\Delta H^0_\alpha = 210$ J/g.

was comparable. Addition of HPN up to a concentration of 0.3% had little effect on the crystallization peaks, Table IV. However, further increasing the concentration of HPN to 0.6% caused a decrease in

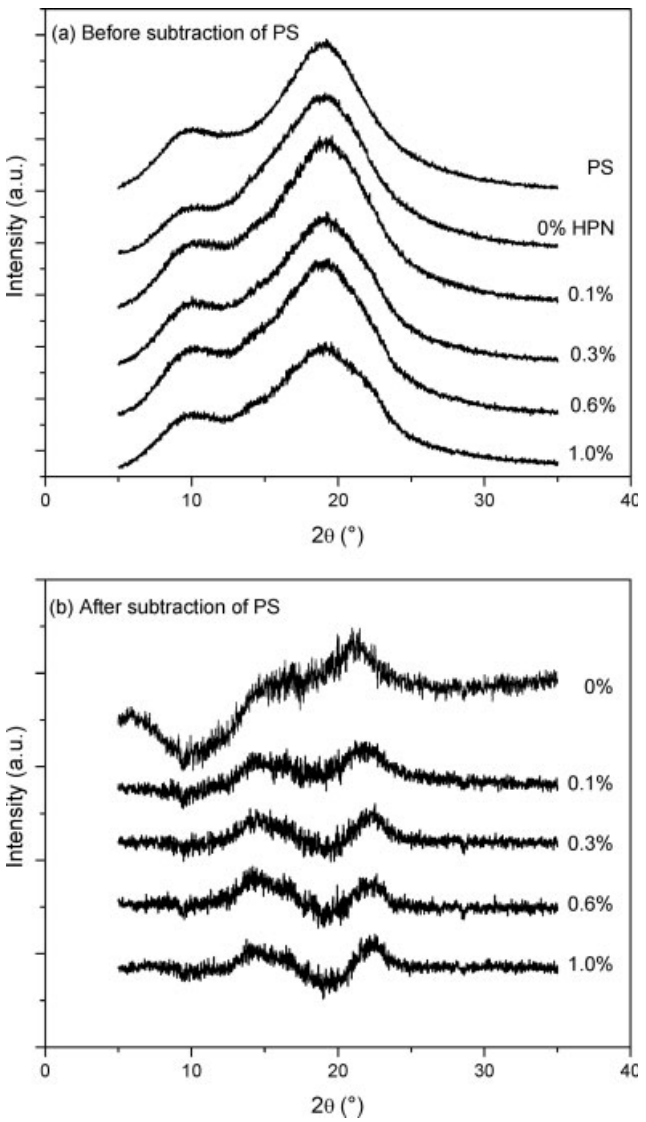

Figure 10 The WAXD curves of the PP particles from 12 nm PP layers with various concentrations of HPN: (a) Before subtraction of the PS contribution; and (b) after subtraction of the PS contribution.

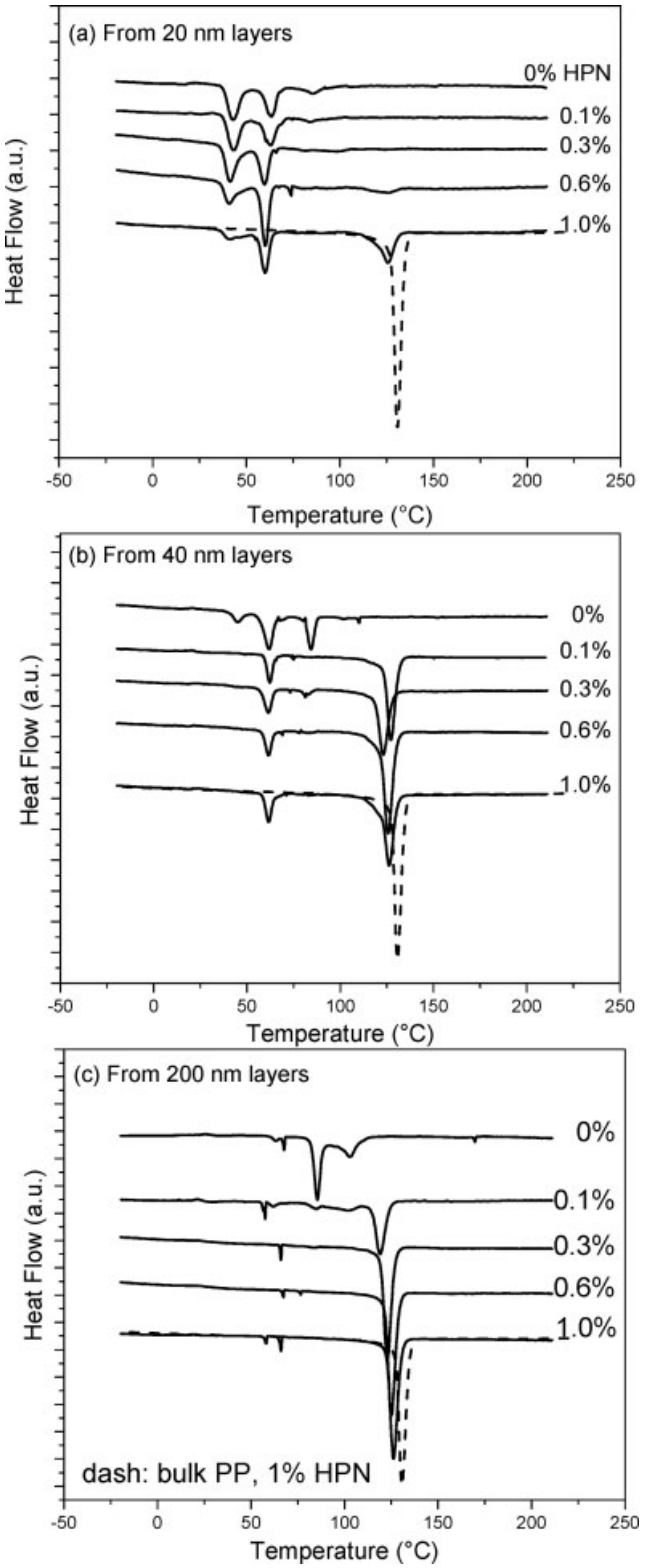

Figure 11 Cooling thermograms of the PP/PS assembly with various concentrations of HPN in the PP layer after heating to 230°C: (a) 20 nm layers; (b) 40 nm layers; and (c) 200 nm layers. The PS contribution was subtracted.

TABLE IV
Crystallization Enthalpies of PP Particles from 20 nm Layers

HPN (wt %)	ΔH_s at 40°C (J/g)	$\Delta H_{\alpha 1}$ at 60°C (J/g)	$\Delta H_{\alpha 2}$ at 85°C (J/g)	ΔH_n at 126°C (J/g)	X_s[a] (%)	X_α[b] (%)	X_{total}[c] (%)
0	26.8	22.6	5.0	0	16	13	29
0.1	25.3	23.1	4.9	0	16	13	29
0.3	27.6	21.3	5.5	0	17	13	30
0.6	18.8	27.9	0	7.0	11	17	28
1.0	13.2	23.9	0	27.9	8	25	33

[a] Calculated from ΔH_s with $\Delta H_s^0 = 164$ J/g.
[b] Calculated from $\Delta H_{\alpha 1} + \Delta H_{\alpha 2} + \Delta H_n$ with $\Delta H_\alpha^0 = 210$ J/g.
[c] Equal to $X_s + X_\alpha$.

the 40°C peak and an increase in the 60°C peak. The same effect was observed when HPN was added to the 12 nm layers. In addition, the peak at 85°C disappeared and a small exothermic peak indicating HPN-nucleated crystallization appeared at 126°C. With 1.0% HPN, the exotherm at 126°C for HPN-nucleated crystallization was much larger. However, even with 1.0% HPN, the peaks at 40 and 60°C remained, although the enthalpies had decreased compared to particles with 0.6% HPN.

Fractionated crystallization of unnucleated PP from 40 nm layers resulted in three crystallization exotherms at 40, 60, and 85°C, Figure 11(b). With only 0.1% HPN, the fractionated crystallization peaks were largely replaced with a large peak at 126°C for nucleated crystallization. The 40°C peak of the homogeneously nucleated smectic form disappeared from the thermogram and the intensity of the 60°C peak of the defective α-form decreased significantly. Moreover, the peak at 85°C in the thermogram of the unnucleated particles was either absent from the thermograms of HPN-nucleated particles or was present as only a small blip on the baseline. The total crystallinity of about 35%, Table V, was higher than the crystallinity obtained with particles from 12 and 20 nm layers, but less than that of the HPN-nucleated PP resin,

The PP particles from 200 nm layers without HPN exhibited three crystallization exotherms at 60, 85, and 102°C, Figure 11(c). With 0.1% HPN in the PP layers, the three lower temperature exotherms were almost gone and an exotherm for nucleated crystallization appeared at 123°C. With higher HPN content, the fractionated crystallization peaks were entirely gone and only a large exotherm at 125°C appeared in the thermogram. The crystallinity of 41%, Table VI, was essentially the same as that of the HPN-nucleated PP resin, indicating that all of the PP in particles was nucleated.

Correlation of fractionated crystallization with particle size

The HPN is a crystalline solid, which is dispersed in the PP melt as micron-sized platelets. The HPN provides a low-energy surface for PP crystals to nucleate. However, in PP nanolayers, the nucleating capacity of HPN is lost. This is inferred from the heating thermograms of the nanolayers. The layers are considerably thinner than the dimension of the HPN platelets and probably the HPN is present as an occasional flaw in the PP nanolayers.

Breakup of PP nanolayers results in a bimodal size distribution of small submicron particles and large micron-sized particles. The fraction of PP as small and large particles depends on the layer thickness, but is not affected significantly on the presence of HPN. The layer breakup process that culminates in the bimodal particle size distribution begins with formation of holes in the thin PP layers. The holes

TABLE V
Crystallization Enthalpies of PP Particles from 40 nm Layers

HPN (wt %)	ΔH_s at 40°C (J/g)	$\Delta H_{\alpha 1}$ at 60°C (J/g)	$\Delta H_{\alpha 2}$ at 85°C (J/g)	$\Delta H_{\alpha 3}$ at 100°C (J/g)	ΔH_n at 126°C (J/g)	X_s[a] (%)	X_α[b] (%)	X_{total}[c] (%)
0	7.3	26.8	18.9	3.9	0	4	22	26
0.1	0	11.7	1.4	0	56.3	0	33	33
0.3	0	13.4	3.3	0	50.2	0	33	33
0.6	0	14.4	0	0	73.3	0	42	42
1.0	0	16.7	0	0	58.9	0	36	36

[a] Calculated from ΔH_s with $\Delta H_s^0 = 164$ J/g.
[b] Calculated from $\Delta H_{\alpha 1} + \Delta H_{\alpha 2} + \Delta H_{\alpha 3} + \Delta H_n$ with $\Delta H_\alpha^0 = 210$ J/g.
[c] Equal to $X_s + X_\alpha$.

can form by amplification of thermal fluctuations at the interface of the thin PP layer and the thick PS layer.[22,23] If a nucleating agent is present, the holes can also form at flaws provided by the HPN platelets. The holes grow and coalesce to form a two-dimensional network defined by thin strings that connect at junction points. If the strings are thin enough, they break up into spherical droplets due to the Rayleigh instability. This is the origin of the small, submicron particles. The network junctions and thicker strings relax into a population of larger droplets. This is thought to be the origin of the bimodal particle size distribution.[17]

It is apparent that the nucleating capacity of HPN is compromised when the PP melt is in the form of dispersed droplets. A comparison of the crystallization thermograms in Figure 12 reveals the persistence of fractionated crystallization in particles from 12, 20, and 40 nm layers, although the amount of fractionated crystallization decreases as the layers become thicker. The decrease in the enthalpy of the fractionated crystallization peaks at 40 and 60°C peaks parallels the decrease in volume fraction of submicron PP particles as observed qualitatively from the OM images alone and as determined semiquantitatively from the combined AFM and OM images. Thus, it appears that HPN does not nucleate crystallization of the small submicron particles. This can be anticipated as the HPN platelets are generally too large to be accommodated within the submicron PP particles. However, the presence of HPN can reduce or eliminate the amount of smectic crystallization at 40°C and can increase the amount of defective α-form crystallized at 60°C. Possibly the HPN contains some contaminate that has a very weak nucleating effect on PP.

In the absence of a nucleating agent, the large PP particles exhibit fractionated crystallization at temperatures lower than 126°C. Fractionated crystallization occurs when the polymer melt is dispersed finely enough that the number of droplets is significantly greater than the number of heterogeneities that are active at low supercooling. In addition, hole formation and breakup can remove contaminants

TABLE VI
Crystallization Enthalpies of PP Particles from 200 nm Layers

HPN (wt %)	Crystallization temperatures (°C)	ΔH_{total} (J/g)	X_α[a] (%)
0	60, 85, 102	72.7	35
0.1	126	75.6	36
0.3	123	81.1	39
0.6	125	85.6	41
1.0	126	86.7	41

[a] Calculated from ΔH_{total} with $\Delta H_\alpha^0 = 210$ J/g.

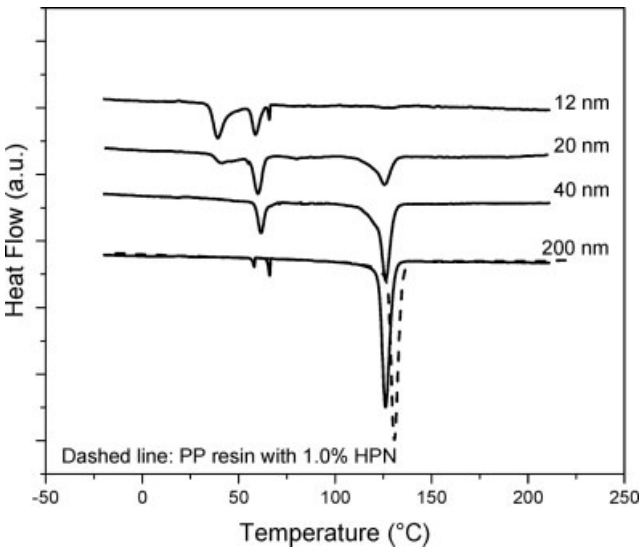

Figure 12 Comparison of the crystallization thermograms of particles from 12, 20, 40, and 200 nm PP layers with 1.0% HPN. The layer thickness is indicated.

that might nucleate crystallization in what is essentially a ''self-cleaning'' process.[24] As a result, some of the HPN may not be available to nucleate crystallization of PP droplets. Nevertheless, at least some of the PP particles from all the layer thicknesses are nucleated by HPN. From the enthalpy of the 126°C peak, only 1% of the PP from 12 nm layers undergoes nucleated crystallization at 126°C. The amount increases to about 33% from 20 nm layers, 65% from 40 nm layers, and 98% from 200 nm layers. Qualitatively, the amount of nucleated crystallization parallels the fraction of PP in the form of large particles. These particles are also large enough to accommodate the HPN platelets.

CONCLUSIONS

A novel application of layer-multiplying coextrusion is to make polymer particles that can be used to study fractionated crystallization. Upon heating assemblies of many PP nanolayers alternating with thicker PS layers into the melt, the thin PP layers breakup to form a dispersion of PP droplets in a PS matrix. The particles that crystallize upon cooling exhibit a bimodal size distribution with one population of small, submicron particles and a second population of large, micron-sized particles. The predominately submicron particles obtained from breakup of 12 nm layers exhibit homogeneous nucleation at about 40°C. As the layer thickness increases, the particle size distribution becomes richer in the larger particles and the particles exhibit multiple crystallization exotherms. The less active nucleation processes responsible for fractionated crystallization are not well understood. We use the opportunity to add

a nucleating agent to the PP nanolayers to probe the effect on crystallization. The presence of the nucleating agent, an organic dicarboxylic acid salt (HPN), does not affect the integrity of the PP nanolayers or the PP particle size distribution resulting from layer breakup. The HPN remains as a crystalline particulate in the melt and provides a low energy surface for crystallization during cooling. It was found that HPN does not nucleate crystallization of the submicron particles, presumably because the HPN platelets are too large to be accommodated within the submicron PP particles. On the other hand, the micron-sized particles, which exhibit fractionated crystallization in the absence of a nucleating agent, are effectively nucleated by the HPN.

References

1. Binsbergen, F. L.; de Lange, M. G. M. Polymer 1970, 11, 309.
2. Kowalewski, T.; Galeski, A. J Appl Polym Sci 1986, 32, 2919.
3. Binsbergen, F. L. Polymer 1970, 11, 253.
4. Thierry, A.; Fillon, B.; Straupé, C.; Lotz, B.; Wittmann, J. C. Prog Colloid Polym Sci 1992, 87, 28.
5. Fillon, B.; Lotz, B.; Thierry, A.; Wittmann, J. C. J Polym Sci Part B: Polym Phys 1993, 31, 1395.
6. Menczel, J.; Varga, J. J Therm Anal 1983, 28, 161.
7. Beck, H. N. J Appl Polym Sci 1967, 11, 673.
8. Thierry, A.; Straupé, C.; Lotz, B.; Wittmann, J. C. Polym Commun 1990, 31, 299.
9. Ghijsels, A.; Groesbeek, N.; Yip, C. W. Polymer 1982, 23, 1913.
10. Morales, R. A.; Arnal, M. L.; Müller, A. J. Polym Bull 1995, 35, 379.
11. Arnal, M. L.; Matos, M.; Morales, R. A.; Santana, O. O.; Müller, A. J. Macromol Chem Phys 1998, 199, 2275.
12. Koutsky, J. A.; Walton, A. G.; Baer, E. J Appl Phys 1967, 38, 1832.
13. Manaure, A. C.; Müller, A. J. Macromol Chem Phys 2000, 201, 958.
14. Santana, O. O.; Müller, A. J. Polym Bull 1994, 32, 471.
15. Bernal-Lara, T. E.; Liu, R. Y. F.; Hiltner, A.; Baer, E. Polymer 2005, 46, 3043.
16. Jin, Y.; Hiltner, A.; Baer, E.; Masirek, R.; Piorkowska, E.; Galeski, A. J Polym Sci Part B: Polym Phys 2006, 44, 1795.
17. Jin, Y.; Hiltner, A.; Baer, E. J Polym Sci Part B: Polym Phys 2007, 45, 1138.
18. Krigbaum, W. R.; Uematsu, I. J Polym Sci Part A: Gen Pap 1965, 3, 767.
19. Bu, H.-S.; Cheng, S. Z. D.; Wunderlich, B. Makromol Chem Rapid Commun 1988, 9, 75.
20. O'Kane, W. J.; Young, R. G.; Ryan, A. J.; Bras, W.; Derbyshire, G. E.; Mant, G. R. Polymer 1994, 35, 1352.
21. Fichera, A.; Zannetti, R. Makromol Chem 1975, 176, 1885.
22. Dutcher, J. R.; Dalnoki-Veress, K.; Nickel, B. G.; Roth, C. B. Macromol Symp 2000, 159, 143.
23. David, M. O.; Reiter, G.; Sitthaï, T.; Schultz, J. Langmuir 1998, 14, 5667.
24. Massa, M. V.; Carvalho, J. L.; Dalnoki-Veress, K. Eur Phys J 2003, 12, 111.